

## **EQUILIBRIUM SATURATION IN BINDER JETTING ADDITIVE MANUFACTURING PROCESSES: THEORETICAL MODEL VS. EXPERIMENTAL OBSERVATIONS**

Hadi Miyanaji\*, Li Yang\*

\*Department of Industrial Engineering, University of Louisville, Louisville, KY40292

### **Abstract**

In Binder Jetting 3D Printing process, a feature is fabricated by depositing binder in the selective regions layer by layer until the geometry is completed. One of the main factors which influences the accuracy and strength of the green parts in this process is the spreading (i.e. lateral migration) and penetration (vertical migration) of the binder in powder bed, which is in turn determined by the capillary equilibrium between the saturated regions and the unsaturated powder. In the present study, a previously developed model for binder migration was applied to 420 stainless steel in order to evaluate the equilibrium saturation levels. Characterizations such as contact angle, specific surface area, suction pressure and capillary pressure were carried out in order to determine the theoretical equilibrium saturation amount. Furthermore, 10 single lines with dimensions of 46 $\mu$ m in diameter and 3mm in length were printed out and analyzed for empirical saturation level. The results of the theoretical model and experimental work were compared and discussed in details to validate its applicability in binder jetting process development.

Keywords: Binder Jetting, 3D Printing, Equilibrium Saturation, Spreading, Penetration.

### **Introduction**

Binder Jetting Additive Manufacturing (BJ-AM) is an additive manufacturing processes in which a liquid binder is deposited through a print-head at the designated locations of the powder bed layer by layer for fabrication of part geometry. After deposition of binder for each layer, the surface of the powder bed is exposed to a fixed amount of heating which is applied via a heat lamp (e.g. infrared heater) so as to partially cure the binder and consequently establish appropriate mechanical strength to withstand the shear and gravitational compressive forces involved in spreading consecutive layers. This layer-by-layer process repeats until the part is completed.

Based on the above description, geometry generation and integrity of the printed part in this process strongly depends upon the interaction between the liquid binder and powder. Once the binder droplets are placed on the selective regions, the liquid binder will migrate into the powder through pores located on the surface of the powder bed (so called imbibition) due to capillary attraction [1-6]. After imbibition is complete (i.e. after all the liquid binder permeates into porous medium), the drainage in which liquid binder migrates from the completely saturated region into the dry powder surrounding it, will begin to take place. Therefore, as binder migration progresses, the saturated regions drain and the dry regions imbibe until capillary pressure of both regions become equal. This is the state where equilibrium condition in which the capillary pressures are equal for both imbibition and drainage, is reached. The saturation level (the ratio of amount of liquid binder to the pore volume in the print material) in the equilibrium phase is of significant

importance in BJ-AM process. This equilibrium saturation must be assumed as the saturation level determined by machine parameters for printing purpose. If the equilibrium saturation is much smaller than the saturation imposed by machine control parameters, the excess liquid binder will tend to migrate out of the designed boundaries of the part. On the other hand, If the equilibrium saturation is much greater than the machine-imposed saturation, the printed part won't have sufficient mechanical strength due to lack of enough amount of binder, which will consequently result in weak bond between the particles and also successive layers. It has been experimentally shown that binder amount plays a major a role in controlling the part accuracy and strength [7-11]. Therefore, it is quite beneficial to be able to predict the equilibrium saturation for a given powder bed and liquid binder using physics-based modeling before the printing process. In the current study, a previously developed model is employed to predict the equilibrium saturation in 420 stainless steel powder bed and the results are compared with empirical measurements of saturation.

One of the few attempts in this regard was reported by J. F. Brecht. In his PhD dissertation conducted at MIT, a model to predict the equilibrium fluid content of printed features from measurements of the capillary characteristics of the powder and physical properties of the fluid binder was developed [12]. It was proposed in this model that a balance of capillary pressure exists between a partially saturated region and the dry powder surrounding the feature. Following this preliminary work, in this paper experimental measurements of the capillary characteristics of the powder were used to calculate the predictions of the equilibrium saturation of the features in order to verify the equilibrium model.

### **The Model**

The interaction between binder and powder in BJ-AM process is dominated by capillary, and to lesser degree, gravitational forces. The liquid binder in the powder bed distributes itself in the pores and contacts the powder surface with a local contact angle of  $\theta$  determined by the surface energies of the solid, liquid, and vapor phase boundaries (see Figure 1). Although the meniscus formed in the vapor-liquid interface may assume a complex profile, it possesses a mean curvature and capillary pressure, defined uniquely everywhere in the binder. On the basis of the Laplace equation, capillary pressure for a local curved interface (local curvature) within a pore is presented by [13]:

$$\Delta p = p_c = \gamma \left( \frac{1}{r_1} + \frac{1}{r_2} \right) \quad (1)$$

where  $\Delta p$  is the capillary pressure across the fluid interface,  $\gamma$  is the surface tension is the  $r_1$  and  $r_2$  are the principal radii of curvature. For a capillary tube of radius  $r$ , the equation (1) becomes as follows [13]:

$$p_c = \frac{2\gamma \cos\theta}{r} \quad (2)$$

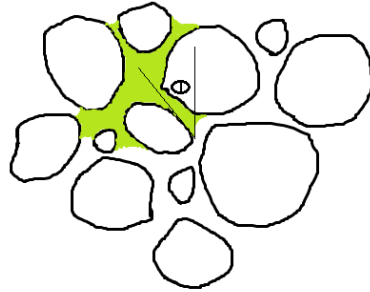


Figure. 1 Local contact angle between liquid binder and a particle in the powder bed

For a real porous material where a liquid binder and powder interact, the outcome of the above equation would be a statistical average which is obtained over the void spaces in the vicinity of the considered pore [14]. From the equation, capillary pressure depends on the geometry of pore, contact angle  $\theta$ , and the degree of saturation ( $S_w$ ). On the other hand, since the relationship of capillary pressure on saturation level ( $p_c = p_c(S_w)$ ) cannot be analytically described due to the shape irregularity and complexity of pores in an actual porous material, laboratory experiments could be implemented to derive the relationship for any given porous media. A typical curve of capillary pressure as a function of saturation is shown in Figure 2.

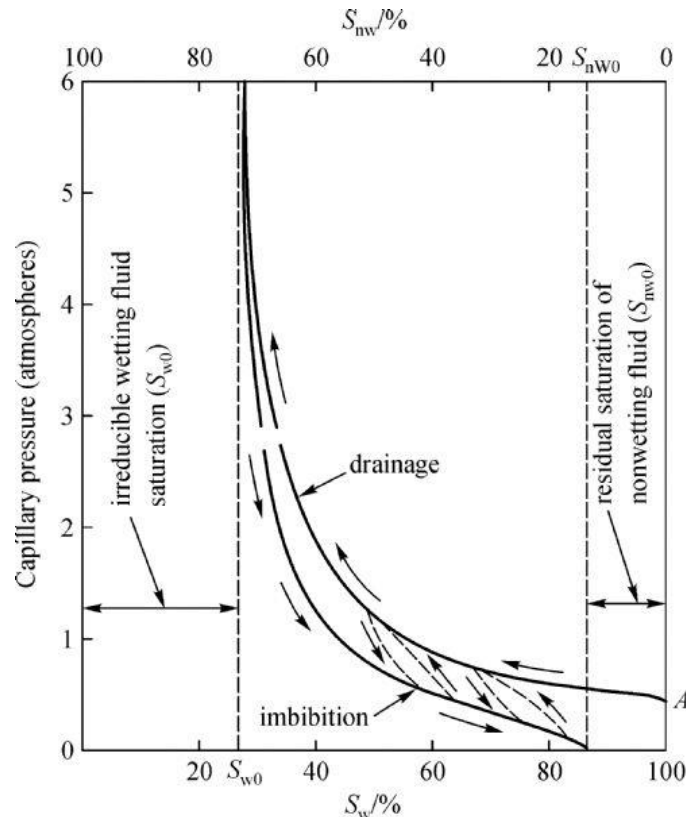


Figure. 2 Typical capillary pressure-wetting fluid saturation curves [12]

From the figure, the curve follows two different paths for imbibition and drainage illustrating hysteresis. The hysteresis in the capillary pressure are known to be rendered by two mechanisms, contact angle ( $\theta$ ) and geometry of void space. While the former depends on the

direction of the displacement, the latter arises from many bottlenecks of pores in the powder bed (ink-bottle effect) [14]. Due to the hysteresis in the capillary pressure curve, the saturated region and dry region the feature can exist at equilibrium with different fluid contents since each of these regions has different pressure characteristics.

There are two important features in Figure 2. Irreducible wetting saturation,  $S_{wo}$ , is a critical wetting fluid saturation at which the fluid displacement in the porous medium approaches zero. The capillary pressure at this saturation is called the dry suction pressure  $P_0$  which is a critical characteristic of a porous medium in determining the liquid binder migration during feature formation in BJ-AM process. The second point in Figure. 2 labelled A on the right side of the graph is the minimum pressure (also called bubbling pressure,  $P_B$ ) required to initiate the displacement of a wetting fluid (e.g. liquid binder) in a fully saturated porous medium.

In the model developed in [10], capillary pressure has been considered as the only driving force for binder migration, and equation (2) was used as the governing relationship between the capillary pressure and liquid binder saturation. In this model, pore curvature ( $K$ ) is defined in such a way that term  $r$  is eliminated from the equation [12]:

$$p_c = \frac{-2\gamma_{LV}\cos\theta}{r} = -K \gamma_{LV} \cos\theta \quad (3)$$

Hysteresis in the capillary pressure between imbibition and drainage of a fluid results in two pore curvature for a single pore and for an assemblage of pores. The critical nonwetting curvature,  $K_{NW}$ , is defined by the bubble pressure,  $P_B$ , and critical wetting curvature  $K_W$  is defined by  $P_0$  as follows [12]:

$$K_W = \frac{2}{R_W} = \frac{-P_0}{\gamma_{LV} \cos\theta_{adv}} \quad (4)$$

$$K_{NW} = \frac{2}{R_{NW}} = \frac{-P_B}{\gamma_{LV} \cos\theta_{rec}} \quad (5)$$

where  $\theta_{adv}$  is advancing contact angle, and  $\theta_{rec}$  is the receding contact angle.

The quantities  $R_W$  and  $R_{NW}$  describe the pore geometry of the powder bed. There two radii are the dimensions of analogous cylindrical capillaries exerting the same capillary pressures as the dry powder and the saturated region, respectively. In Fredric's model, a fully saturated feature is modelled as a cavity with two capillaries, one with radius  $R_W$  that represents the path of dry pores that lead out into bulk powder bed, and the other one with a radius  $R_{NW}$  that represents the trail of the saturated pores that guide air into the feature [12].

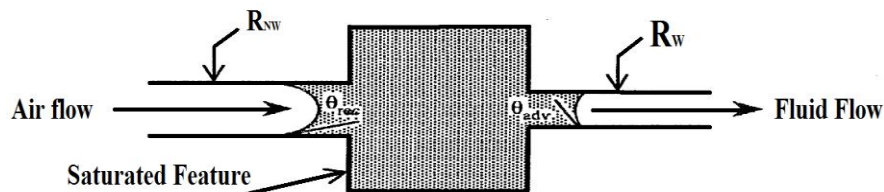


Figure. 3 The model for equilibrium of a liquid binder in a hydraulic feature [10]

Liquid pressure can be transmitted across this feature. Besides fully saturated regions, pores that have been partially drained but still in hydraulic contact are included in this model.

If the pressure within the larger capillary ( $R_{NW}$ ) is greater than that of smaller capillary in Figure 3, fluid will spontaneously migrate from left to right. In the current model, the excess pressure in the feature is expressed in terms of the differences in the pressure between two capillaries [12]:

$$\Delta P = -P_0 + P_B \quad (6)$$

In terms of the critical radii becomes

$$\Delta P = 2\gamma_{LV} \left[ \frac{\cos\theta_{adv}}{R_W} - \frac{\cos\theta_{rec}}{R_{NW}} \right] \quad (7)$$

Or alternatively,

$$\Delta P = \gamma_{LV} [K_W \cos\theta_{adv} - K_{NW} \cos\theta_{rec}] \quad (8)$$

This excess pressure is driving force for fluid migration in a porous medium. Liquid binder which is often employed in printing process is highly wetting to the powder (i.e.  $\cos\theta_{adv} \approx \cos\theta_{rec} \approx 1$ ). Under these circumstances, the difference in critical pore curvatures ( $K_W - K_{NW}$ ) defines the driving force for binder permeation out of a fully saturated region. As a feature becomes less than fully saturated, the excess capillary pressure is proportional to the difference  $[K_W \cos\theta_{adv} - K_{drainage} \cos\theta_{rec}]$  where  $K_{drainage}$  is dependent on the saturation. Therefore, the condition for hydrostatic equilibrium of a feature is

$$K_{drainage}(S^*) = K_W \quad (9)$$

where  $S^*$  is the equilibrium saturation.

Therefore, given the powder bed and liquid binder characteristic such as the suction pressure, the capillary pressure curves, surface tension, contact angle, etc. it is possible to estimate the equilibrium saturation of a printed feature using the relationship by Eq.(9).

### **Methodology**

In this study, ExOne M-Lab machine was used for printing 420 Stainless steel samples. As shown in figure 4, particle size of the used powder varies between 10 $\mu$ m and 40 $\mu$ m. The packing density of the powder was measured to be 55% once spread with the traverse rate of 3mm/sec. In order to measure the experimental equilibrium saturation, some cylindrical specimens were printed out and their dimensions were measured using an optical microscope. For all the samples, process parameters 100% saturation level, 70% curing power intensity, 45 sec curing time, and 3mm/sec spreading speed were employed.

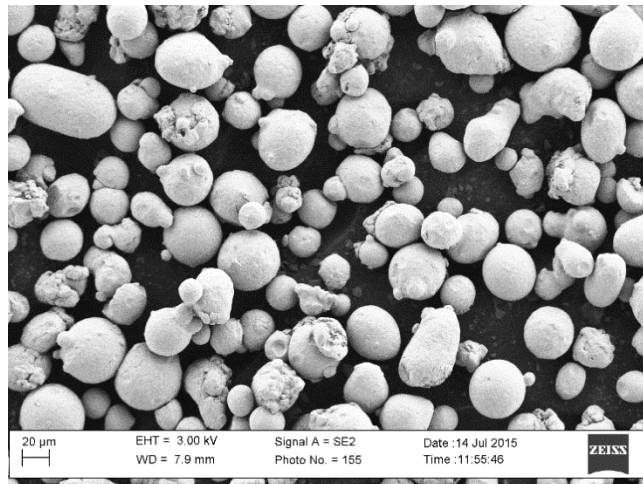


Figure. 4 The morphology of 420 Stainless steel

In order to determine the theoretical equilibrium saturation, the powder and liquid binder characteristics (e.g. liquid binder surface tension and viscosity, contact angle, specific surface area of the powder, and capillary pressure-saturation curve) need to be specified. The Cannon-Fenske Routine Viscometer, size 150, was employed to measure the viscosity of the liquid binder according to ASTM D445 and ISO 3104 [15]. For determining the surface tension of the binder, stalagmometric method was chosen. In this method, the total weight and number of drops of the liquid binder falling from a capillary glass tube (figure 5) were recorded, and the surface tension of the fluid were consequently calculated.



Figure. 5 Volumetric pipet used for measuring the surface tension of the binder

The specific surface area of the powder was determined using BET (Brunauer, Emmett and Teller) method. The principle of this method is based upon physical adsorption of a gas on the surface of the solid and by calculating the amount of adsorbate gas corresponding to a monomolecular layer on the surface. For this purpose, commercial TriStar 3000 device was utilized.

Capillary Penetration Method is widely used for average contact angle determination applying the Washburn equation. In this method, the mass of liquid binder absorbed into the porous medium is recorded as a function of time. The contact angle can then be derived from the modified Washburn theory [1, 16, 17]:

$$m^2 = \frac{C \rho^2 \gamma_{lv} \cos\theta}{\eta} t \quad (10)$$

where  $m$  is the mass increase of the column,  $t$  is time,  $\gamma_{lv}$  is the binder surface tension,  $\eta$  is the binder viscosity,  $\rho$  is the binder density, and  $C$  is the capillary constant. The capillary constant  $C$  can be determined using the following relationships [16].

$$C = \frac{r \pi^2 R_k^4 \varepsilon^2}{2} \quad (11)$$

where  $r$  is the pore radius,  $R_k^4$  is the radius of the capillary tube (figure 6),  $\varepsilon$  is the porosity of the powder pack.

The effective radius,  $r_{eff}$ , (Eq. 12), can be replaced with  $r$  in the equation above [16]

$$r_{eff} = \frac{2(1-\phi)}{\phi \rho A} \quad (12)$$

where  $\phi$  is the volume fraction of solid in the tube,  $\rho$  is the density of the solid material, and  $A$  is the specific surface area per gram of solid (obtained from BET measurement).

The apparatus for the Capillary Penetration experiment is shown in the Figure below. The powder particles were poured into a glass capillary (0.56 cm inner diameter and 7 cm long) which was supported at the bottom by Humboldt filter paper. The decrease in mass of the container (owing to the liquid binder permeation upward into the capillary) was recorded using an electronic balance as a function of time. The time  $t = 0$  corresponds to the instant of capillary tube submersion in the liquid binder. After the binder mass was sucked into the capillary glass tube, packing density of the bed, and specific surface area of solid, average contact angle was then calculated.

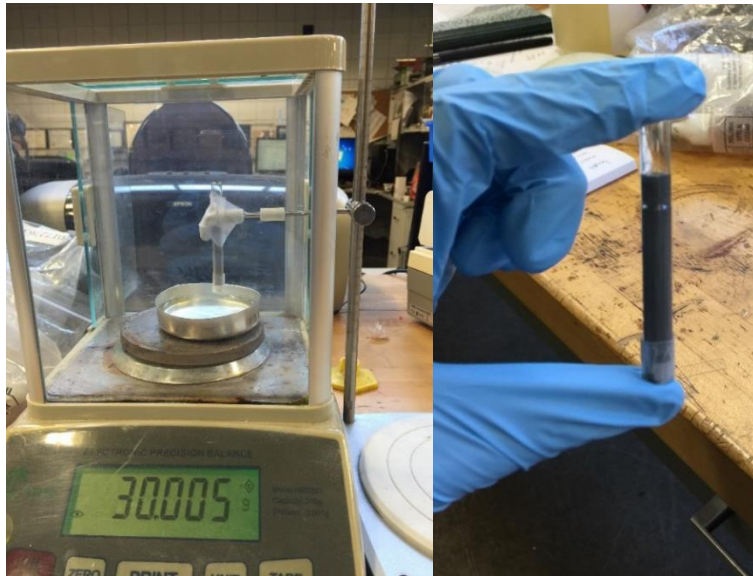


Figure 6. Apparatus used for Capillary Penetration experiment

The rate of imbibition measured can be also used to determine the dry capillary pressure according to Washburn equation:

$$x^2 = \frac{2K_{sat} P_0}{\varepsilon \eta} t \quad (13)$$

where  $x$  is the distance of the penetration front from the contact point,  $\varepsilon$  is the porosity of the sample,  $\eta$  is the viscosity of the liquid binder,  $K_{\text{sat}}$  is the hydraulic permeability, and  $P_0$  is the dry suction pressure.

For measuring the hydraulic permeability,  $K_{\text{sat}}$ , in the above formulation a set up shown in figure 7 was used. The tube is secured in the bottom end and filled with a liquid on top of the sample. In this experiment, if the height is measured over time, an equation of the following form can be employed to determine the hydraulic permeability.

$$h = h_0 e^{-nkt} \quad (14)$$

where  $k$  is the permeability,  $L$  is the sample thickness,  $A$  is the sample cross-section,  $r$  is the inside radius of the tube, and  $n$  is a geometrically determined constant which is defined as

$$n = A/\pi r^2 L \quad (15)$$

where  $h_0$  corresponds to the initial height of binder at time 0.

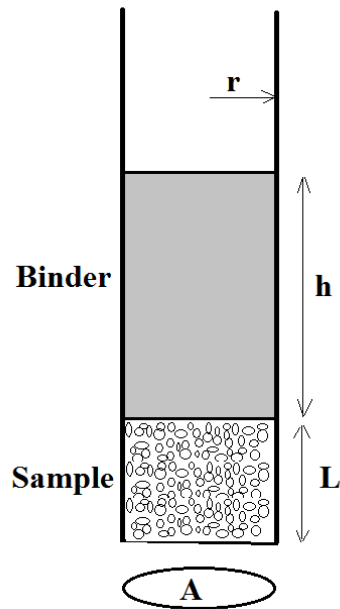


Figure 7. Schematic diagram of the set up for hydraulic permeability measurement

Lastly, filter paper method was used to obtain the capillary pressure-saturation curve in drainage [18]. This method was initially developed in the soil science for measuring soil suction. The filter paper method is cheap, simple, and capable of covering the entire range of suction pressures [19]. The testing method is based the assumption that a filter paper will achieve equilibrium with a sample having a specific suction by either liquid or vapor moisture exchange between the sample and the filter paper. Once equilibrium is achieved, the water content of the filter paper will correspond to suction pressure through filter paper calibration curve shown in Figure 8. For the present study, samples of 0%, 10%, 30%, 45%, 60%, 80, 90%, and 100% saturation levels were prepared, and their corresponding capillary pressure were calculated using

the water content of the filter papers after equilibration according to ASTM D5298-10. Thereafter, the capillary pressure-saturation curve was plotted with these data. It is of interest to note that capillary pressure corresponding 0% saturation level denotes the dry suction pressure described previously.

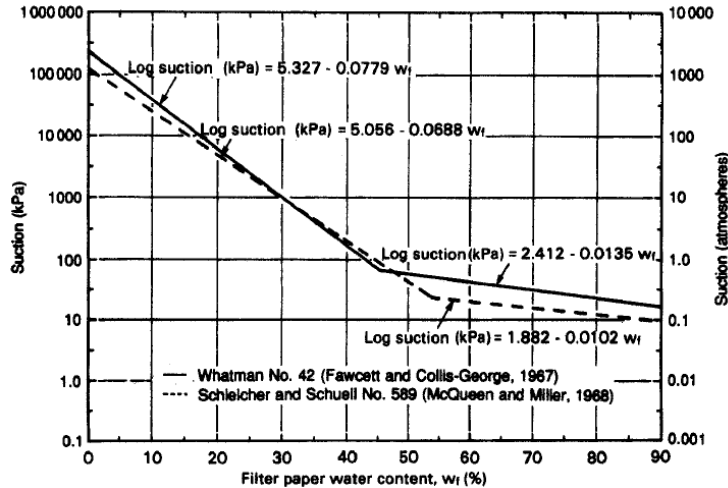


Figure. 8 Calibration curves for two types of filter paper [18]

### Result and discussion

The results of filter paper method were converted to equivalent pore curvatures and displayed in Figure 9. This plot shows how the pore curvature defined previously varies with saturation amount introduced into the 420 stainless steel.

Table 1 summarizes the results of different methods employed for characterizing the binder and powder interaction. These outcomes were then used to calculate the dry suction pressure,  $P_0$ , and the average contact angle between powder particles and the liquid binder permeating the powder bed.

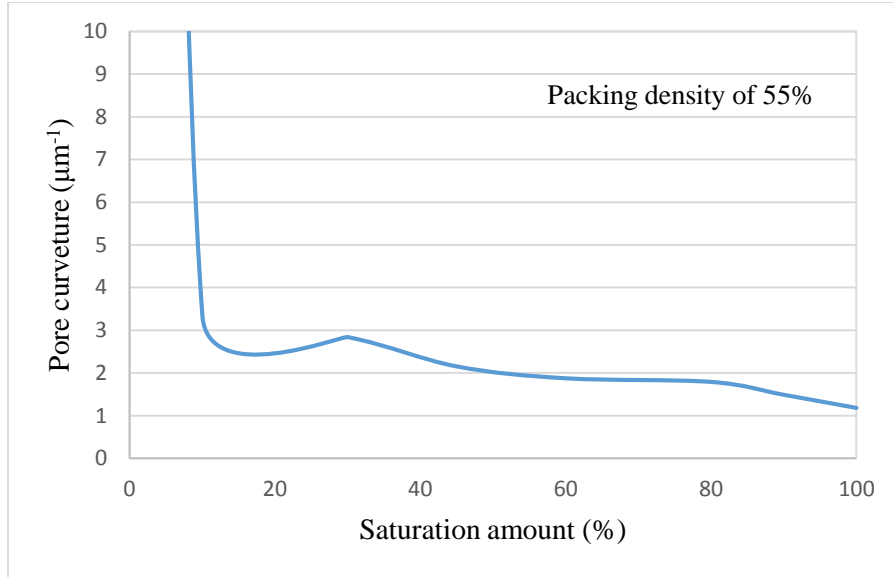


Figure. 9 The capillary pressure-saturation curve in drainage

Table. 1 summary of the results

Method	BET	The Cannon-Fenske Routine Viscometer	Stalagmometric method
Factor measured	Specific surface area (m <sup>2</sup> /g)	Viscosity of the binder used (Pa.s)	surface tension of the binder (N/m)
Results	0.03	0.00431	0.03

From the capillary penetration measurements, it was found out that the penetration rate (imbibition rate) and the hydraulic permeability ( $K_{sat}$ ) of the powder bed were  $0.02 \text{ cm}^2/\text{s}$  and  $1.3 \times 10^{-9} \text{ cm}^2$  respectively. Therefore, according to the Washburn equation (Eq. 13) the dry suction pressure  $P_0$  was calculated as [1]:

$$P_0 = \frac{2.7 \times 10^{-5}}{1.3 \times 10^{-9}} = 2 \times 10^4 \text{ Pa} = 21 \text{ kpa}$$

Also, given  $\phi = 0.55$ ,  $\rho = 7.74 \frac{\text{g}}{\text{cm}^3}$ , and  $A = 0.03 \text{ m}^2/\text{g}$ ,  $\varepsilon = 0.45$  the effective radius,  $r_{eff}$ , and the capillary constant  $C$  were determined as:

$$r_{eff} = \frac{2(1-\phi)}{\phi \rho A} = \frac{2(1-0.55)}{0.55 \times 7.74 \times 0.03} \times 10^{-6} = 6.8 \times 10^{-6} \text{ m}$$

$$C = \frac{6.8 \times 10^{-6} \pi^2 (0.29)^4 (0.45)^2}{2} = 4.8 \times 10^{-16} \text{ m}^5$$

Similar to the original form of Washburn equation [1], which represents linear dependence of square of height versus time, the modified Washburn equation (Eq. 10) [16,17] also shows linear trend of binder mass square versus time as shown in Figure 10. This kind of phenomenon has been empirically observed by many researchers [17,20,21]. The dotted line in Figure 9 corresponds to the  $y^2 = At$  trend-line, where  $A$  is a fitting parameter defined as  $A = \frac{C \rho^2 \gamma_{lv} \cos \theta}{\eta}$ . Given  $A = 0.0017 \text{ g}^2/\text{sec}$  according to Figure 9 and the capillary constant  $C = 4.8 \times 10^{-16} \text{ m}^5$ , the average contact angle between the liquid binder and particles in the powder bed can be calculated as:

$$\cos\theta = \frac{A \eta}{c \rho^2 \gamma_{lv}} = \frac{0.0017 \times .00431}{4.8 \times 10^{-16} \times 10^{12} \times 0.03} = 0.5 \Rightarrow \theta = 60^\circ$$

This amount is well within the range reported in the literature for the contact angle of stainless materials with liquids similar to the used binder in the present study in terms of physical properties [22, 23].

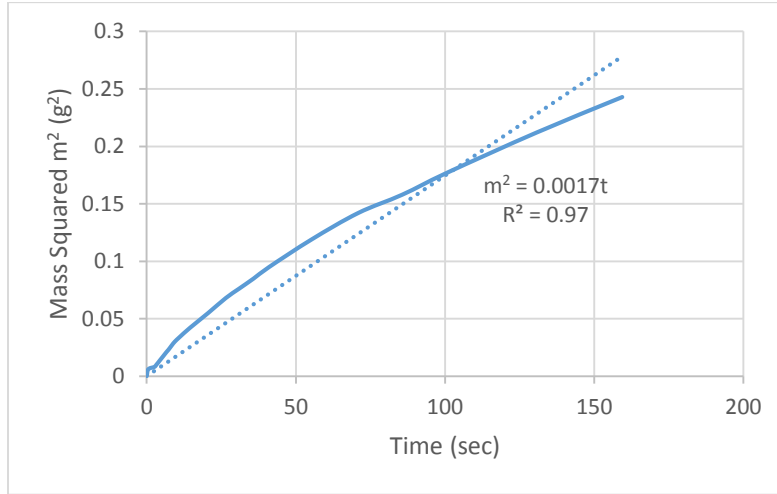


Figure. 10 The binder mass absorbed versus time

Finally, the equilibrium saturation could be determined using Eq.(9) as follows:

$$K_{drainage}(S^*) = K_W = \frac{-P_0}{\gamma_{LV} \cos\theta_{adv}} = 1.4 \mu m^{-1}$$

From the capillary pressure-saturation curve, this pore curvature which corresponds to the equilibrium saturation amount can be observed at a saturation level of approximately 85%. The saturation obtained represents the theoretical binder amount present in the equilibrium condition. Further saturation measurements are required be performed to evaluate the accuracy of the model.

To determine the empirical equilibrium saturation, 10 single lines, with the diameter of 46  $\mu m$  and length of 3mm, were printed out with process settings of 100% saturation level, 70% power intensity, 45sec for curing time, and 2 mm/s as spread speed. The diameters of the lines were measured by optical microcopy. Figure 11 displays two examples of the printed features.

Given the packing density of the powder bed, the binder density, the binder amount deposited from the machine settings, and having measured the dimensions of the printed features, the equilibrium saturation can be determined as the ratio of binder amount deposited to the pore volume present in the fabricated features. In the present study, ratio was measured to be 60% representing the equilibrium saturation in practice.

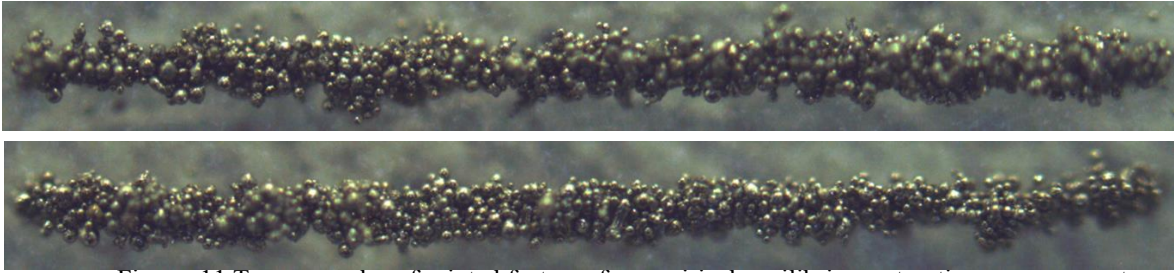


Figure. 11 Two examples of printed features for empirical equilibrium saturation measurements

The results reveals that the equilibrium saturation estimate from the capillary pressure measurements varies by 29% from the empirical saturation obtained from experimental measurements. This discrepancy might be explained as follows.

In the current model, capillary pressure/saturation curve *in drainage* is used to determine the final saturation amount using the dry suction pressure which will always lead to higher saturation level. In the equilibrium state there exists a trail of partially saturated pore with an irreducible wetting saturation level where the liquid binder ceases to migrate. The simplest case of this phenomenon is shown in Figure 12 with only two pores. In this picture, pore 1 drains and pore 2 imbibe until the capillary pressures between two pores become equal. The capillary pressure corresponding to pore 2 is referred to as irreducible wetting saturation. Due to the capillary pressure hysteresis between drainage and imbibition, if the capillary pressure characteristic curve *in drainage* is used for predicting the equilibrium saturation (which is the case in the model), this estimate will always be higher than actual saturation.

The other factor which might be contributing to higher estimate of equilibrium saturation is neglecting gravity effect particularly in the vertical direction. The effect of gravity on the hydrostatic pressure within a feature can cause fluid to flow further downward out of the boundaries. Consideration of gravity effect in the model will result in higher driving pressures for binder migration which in turn lead to lower estimate of the saturation in the equilibrium condition.

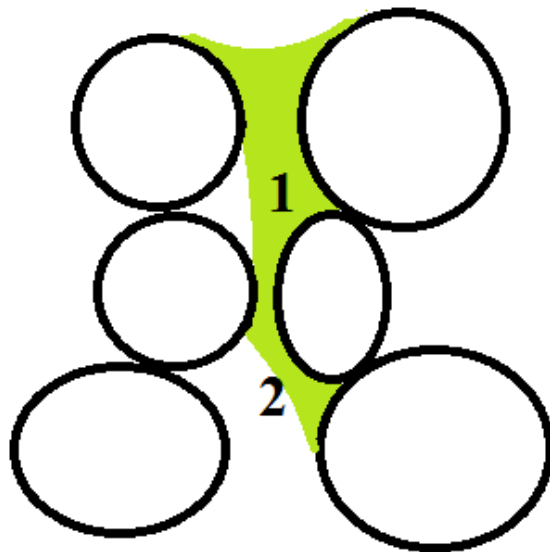


Figure. 12 Equilibrium state of two partially saturated pores

## **Conclusion**

In 3D printed features using Binder Jetting process, there exists an equilibrium condition in which the liquid binder ceased to migrate due to the balance between the capillary pressures of saturated regions and unsaturated ones. The saturation level in this state (also called equilibrium saturation) plays an important role in dimensional accuracy, integrity, and strength of the printed parts. In the present work, a previously developed model of binder migration was applied to 420 stainless steel in order to evaluate the equilibrium saturation levels. Different powder and binder characterizations such as contact angle, specific surface area, dry suction pressure and capillary pressure curve, were performed as to calculate the theoretical equilibrium saturation amount. Additionally, in order to determine the equilibrium saturation in practice 10 single lines were printed out and analyzed using an optical microscope. The results showed that the equilibrium saturation estimated from the capillary pressure measurements varies by 29% from the empirical saturation obtained from experimental measurements. Using capillary pressure/saturation curve *in drainage* and also neglecting the gravity effect in the model might be two contributing factors to a higher estimate of equilibrium saturation.

## **Acknowledgement**

The authors also express their gratitude to the staff of Rapid Prototyping Center and Conn Center at the University of Louisville for their assistance and also Dr. Samuel Dilip for the help on performing this project.

## References

- [1]. E. W. Washburn (1921), The dynamics of capillary flow, *Phys. Rev.*, 17: 273 – 283.
- [2]. A. MARMUR (1988), Penetration of a Small Drop into a Capillary, *Journal of Colloid and Interface Science*, Volume 122, Issue 1, Pages 209-219
- [3]. A. MARMUR (1988), Drop Penetration into a Thin Porous Medium, *Journal of Colloid and Interface Science*, Volume 123, Issue 1, May 1988, Pages 161-169
- [4]. S. Levine, G. Neal (1975), Theory of the rate of wetting of a porous medium, *J. Chem. Soc., Faraday Trans. 2*, 1975,71, 12-21
- [5]. H. Miyajima, S. Zhang, A. Lassell, A. Zandinejad, L. Yang, “Process Development of Porcelain Ceramic Material with Binder Jetting Process for Dental Applications”, *The Journal of The Minerals, Metals & Materials Society (TMS)*, 2016, 68: 831
- [6]. H. Miyajima, S. Zhang, A. Lassell, A. A. Zandinejad, L. Yang (2015), Optimal process parameters for 3D printing of dental porcelain structures, *proceedings of the 24th International Solid Freeform Fabrication Symposium*. Austin, TX, USA.
- [7]. M. Vaezi & C. K. Chua (2010), Effects of layer thickness and binder saturation level parameters on 3D printing process. *Int J Adv Manuf Technol* (2011) 53:275–284
- [8]. S.M. Gaytan, M.A. Cadena, H.Karim, D.Delfin, Y.Lin, D.Espalin, E. MacDonald, R.B.Wicker (2015), Fabrication of barium titanate by binder jetting additive manufacturing technology, *Ceramics International*41(2015)6610–6619
- [9]. Gu, H., Gong, H., J.J.S. Dilip, Pal, D., Hicks, A., Doak, H., & Brent Stucker (2015), “Effects of Powder Variation on the Microstructure and Tensile Strength of Ti-6Al-4V Parts Fabricated by Selective Laser Melting,” *International Journal of Powder Metallurgy*, Winter issue, pp. 35-42.
- [10]. K. Lu, W. T. Reynolds (2008), 3DP process for fine mesh structure printing, *Powder Technology* 187 (2008) 11–18
- [11]. P. Deepankar, N. Patil, M. Nikoukar, K. Zeng, K. H. Kutty, and B. E. Stucker (2013), "An integrated approach to cyber-enabled additive manufacturing using physics based, coupled multi-scale process modeling." In *Proceedings of SFF Symposium*, Austin, TX.
- [12]. J. F. Brecht (1995), *Binder Stability and Powder\Binder Interaction in Three Dimensional Printing*, PhD dissertation conducted at MIT.
- [13]. J. H. Weaver (Ed.) (1987), *The world of physics: a small library of the literature of physics from antiquity to the present*, Simon & Schuster, New York, pp. 579–582
- [14]. J. Bear (1972), *Dynamics of fluids in porous media*, Elsevier, New York.
- [15]. ASTM D445, *Standard Test Method for Kinematic Viscosity of Transparent and Opaque Liquids (and Calculation of Dynamic Viscosity)*, ASTM Volume 05.01 Petroleum Products, Liquid Fuels, and Lubricants (I): C1234-D3710
- [16]. T. Da. Vu, J. HUPKA (2005), *Characterization of Porous Materials by Capillary Rise Method*, *Physicochemical Problems of Mineral Processing*, 39, 47-65
- [17]. J. Shang, M. Flury, J. B. Harsh, R. L. Zollars (2008), Comparison of different methods to measure contact angles of soil colloids, *Journal of Colloid and Interface Science* 328: 299–307
- [18]. ASTM D5298-10, *Standard Test Method for Measurement of Soil Potential (Suction) Using Filter Paper*, ASTM Volume 04.08 Soil and Rock (I): D420-D5876
- [19]. D. G. Fredlund, H. Rahardjo (1993), *Soil Mechanics for Unsaturated Soils*, ISBN-13: 978-0471850083
- [20]. A. Siebold, M. Nardin, J. Schultz, A. Walliser, M. Oppliger (2000), Effect of dynamic contact angles on capillary rise phenomena, *Colloid Surf. A*, 161(1): 81 – 87.

- [21]. E. Chibowski, L. Holysz (1992), Use of the Washburn equation for surface free energy determination, *Langmuir*, 8710 – 716.
- [22]. S. G. Kandlikar, M. E. Steinke (2002), Contact angles and interface behavior during rapid evaporation of liquid on a heated surface, *International Journal of Heat and Mass Transfer* 45: 3771–3780
- [23]. S. G. Kandlikar, M. E. Steinke (2001), Contact Angles of Droplets During Spread and Recoil After Impinging on A Heated Surface, *Trans IChemE*, Vol 79, Part A,